A dual-beam lens-free slot-array antenna coupled high-T_c superconducting fundamental mixer at the W-band

Xiang Gao[1,2], Ting Zhang[3], Jia Du[2], Jianping An[1], Xiangyuan Bu[1] and Jay Guo[3]

[1] School of Information and Electronics, Beijing Institute of Technology, Beijing 100081, People's Republic of China
[2] Commonwealth Scientific and Industrial Research Organisation (CSIRO) Manufacturing, Lindfield, NSW 2070, Australia
[3] Global Big Data Technologies Centre, University of Technology Sydney, Ultimo, NSW 2007, Australia

E-mail: gaox@bit.edu.cn, Ting.Zhang@uts.edu.au

Received xxxxxx
Accepted for publication xxxxxx
Published xxxxxx

Abstract

This paper presents a W-band high-T_c superconducting (HTS) Josephson-junction fundamental mixer which is coupled using a dual-beam lens-free slot-array antenna. The antenna features a uniplanar six-element slot array fed by an ungrounded coplanar waveguide line, of which each element is a long slot loaded by four rectangular loops. Highly directional radiation is therefore realized by utilizing the long slots and array synthesis to form a relatively large antenna aperture. The antenna also enables asymmetric dual-beam radiation in opposite directions, which not only reduces the RF coupling losses but greatly facilitates the quasi-optics design for the integration of the HTS mixer into a cryocooler. The electromagnetic simulations show that a coupling efficiency as high as -2.2 dB, a realized gain of 13 dB and a front-to-back ratio of 10 dB are achieved at the frequency of 84 GHz. Using this on-chip antenna, a W-band HTS fundamental mixer module is experimentally developed and characterized for different operating temperatures. The measured conversion gain is -10 dB at 20 K and -14.6 dB at 40 K, respectively. The mixer noise temperature is predicted to be around 780 K at 20 K and 1600 K at 40 K, respectively. It is also analyzed that the mixer performance can be further improved if the Josephson junction parameters were optimized.

Keywords: W-band fundamental receiver, high-T_c superconducting Josephson junction, slot-array antenna, asymmetric dual beam, millimeter-wave communication.

1. Introduction

Millimeter-wave (MMW) regions (30-300 GHz) have increasingly been exploited for applications in gigabit-per-second wireless communications [1], high-resolution imaging [2] and astronomy [3]. In addition to higher data-rates, MMW communications bring additional advantages compared with the microwave links, such as smaller system volume and lighter user terminals. The combined merits in resolution and penetrability make the MMW imagers very promising for security inspection and non-destructive testing. MMW frequencies also bring abundant spectral information

for astronomical observation. Unfortunately, the huge potential at MMW frequencies comes with a cost. MMW wireless systems suffer from limited transmitting power and severe atmospheric attenuation, which is particularly severe at higher MMW frequencies such as 70/80GHz, or W-band. One solution to address the challenge is to employ sensitive heterodyne receiver frontend technologies.

MMW heterodyne receivers have been developed by using the semiconductor [4], low-T_c superconducting (LTS) [3] and high-T_c superconducting (HTS) Josephson [5-10] technologies. Semiconductor receivers are advantageous for the capability of room-temperature operation, while superconducting receivers are more promising for their superior detection sensitivity and lower local-oscillator (LO) power requirement. Compared to the LTS counterparts, HTS Josephson receivers can operate in single-stage miniature commercial cryocoolers thus significantly reducing the system volume and cryogenic cost. For superconducting receivers operating above 50 GHz, the radio-frequency (RF) and LO signal coupling are critically important as they directly influence the conversion and noise performance. Considering the technical difficulties in precise machining and thermal isolation of the cryocooler feedthrough for waveguide coupling, quasi-optical coupling is a preferred solution for superconducting receivers due to ease of fabrication with relatively low cost.

The quasi-optically coupled receiver generally employs a planar thin-film antenna integrated with a dielectric lens to increase the radiation directivity and gain. Typical log-periodic [11] and spiral [8] antennas are broadband radiators with stable characteristics over a wide frequency range, while exhibiting poor coupling efficiency for those superconducting devices of low junction impedance. In comparison, narrowband twin-slot [12] and ring-slot [13] antennas are easier to be designed for low-impedance matching and high-efficient coupling. A high-performance dual-band on-chip antenna [14] also has been developed for the HTS fourth-harmonic mixing application. It should be mentioned that despite those achievements, such integrated lens antenna is not so appropriate for 70/80-GHz receivers. This is mainly due to the fact that the large volume of dielectric lens increases not only the RF propagation loss but also assembly difficulty and instability. Furthermore, since there is only one single beam for those reported antennas, a beam splitter must be utilized for combining the RF and LO signals before coupled into the superconducting receiver, thus complicating the quasi-optical configuration and alignment adjustment. Although a 300-GHz dual-beam antenna had previously been reported [15], it was designed using the dielectric lens unsuitable for the 70/80-GHz band. Besides, the antenna features small beam separation angle of only 40° [15], which is still inconvenient for the quasi-optical configuration.

In this work, we present a dual-beam lens-free slot-array antenna coupled HTS Josephson fundamental mixer operating at the W-band. The antenna can greatly reduce the RF coupling loss and simplify the quasi-optical configuration for HTS receiver integration. Our major innovative contributions are highlighted below. (1) A uniplanar dual-beam lens-free slot-array antenna was proposed and designed for superconducting receivers, which utilizes the rectangular-loop loaded slots and array synthesis to realize asymmetric dual-beam radiations in opposite directions. Specific theoretical analyses were conducted to clarify the designs for radiation pattern optimization, impedance matching and surface wave suppression. (2) A prototype of the slot-array antenna coupled W-band HTS fundamental mixer was developed. The mixer was fabricated, packaged, and experimentally characterized for different operating temperatures. The measured results agree well with that from numerical simulation, which have shown the good device performance and validated the effectiveness of our antenna design.

2. Dual-beam lens-free slot-array antenna

Fig. 1 shows the geometry of a W-band dual-beam lens-free slot-array antenna. The antenna is comprized of long radiating slots, coplanar waveguide (CPW) feeding lines and a CPW choke filter, all of which are patterned on the top gold film layer of a MgO chip. The main radiator is a CPW fed slot array with six elements, where each element consists of five slot sections and four rectangular loops. Compared to the conventional radiating slot with shorter length, the utilization of a long radiating slot with multiple slot sections helps to extend the magnetic current path thus enlarging the radiating aperture in the X direction. It is known from the resonant radiation mechanism that there would appear reverse magnetic currents on an unloaded long slot, which inevitably deteriorates the radiation patterns. With the aim of achieving broadside radiation beams, four rectangular loops are loaded on both sides adjacent to the slot sections for eliminating reverse magnetic currents or electric fields on all slot sections. By tuning and optimizing the lengths of the slot sections and rectangular loops, the reversed currents are controlled to concentrate only on the loops, which contribute very little to radiation due to mutual cancellation. For array synthesis in the Y direction, the CPW meander lines with one effective wavelength are utilized to realize in-phase excitation for six elements. The slot array antenna is implemented on an MgO substrate which is required for the HTS junction technology using a $YBa_2Cu_3O_{7-x}$ (YBCO) thin film. The gold film on top layer is extended into the backside of the substrate with two shorting walls, which can be tightly attached to the packaging house (using the silver epoxy) to form a ground for dc biasing and measurement. Considering the resonant radiation mechanism of the slot-array antenna, a

CPW fourth-order stepped-impedance choke filter is utilized for preventing the leakage of RF and LO electric currents into the dc/IF port. Using this antenna, the incident RF and LO signals can be quasi-optically coupled into a superconducting Josephson junction located at the antenna port (i.e., in between the CPW feeding lines). After heterodyne mixing between those two signals inside the junction, the down-converted intermediate-frequency (IF) signal can be output from the dc/IF port (shared by dc biasing) at the leftmost end of the MgO chip.

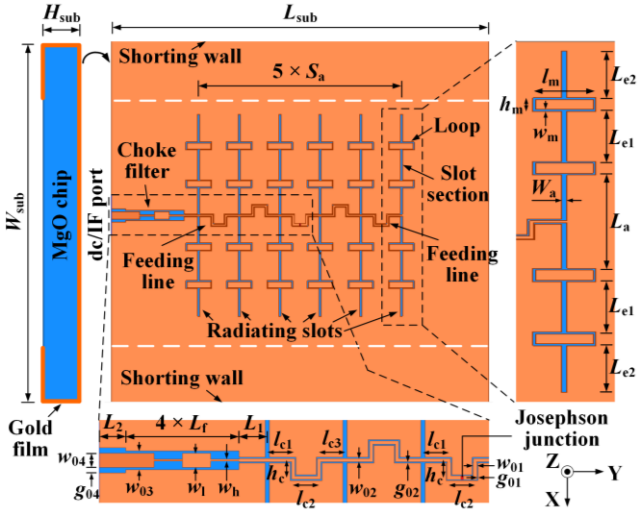

Fig. 1. Geometry of a W-band dual-beam lens-free slot-array antenna (H_{sub} = 0.3 mm, L_{sub} = 10 mm, W_{sub} = 10 mm, S_a = 1.074 mm, W_a = 30 μm, L_a = 1.5 mm, L_{e1} = 0.82 mm, L_{e2} = 0.75 mm, l_m = 0.656 mm, h_m = 0.185 mm, w_m = 15 μm, L_1 = 0.39 mm, L_2 = 0.365 mm, L_f = 0.39 mm, l_{c1} = 0.358 mm, l_{c2} = 0.358 mm, l_{c3} = 0.358 mm, h_c = 0.25 mm, w_{01} = 46 μm, g_{01} = 4 μm, w_{02} = 30 μm, g_{02} = 12 μm, w_{03} = 0.27 mm, w_{04} = 0.254 mm, g_{04} = 80 μm, w_h = 16 μm, and w_l = 0.254 mm).

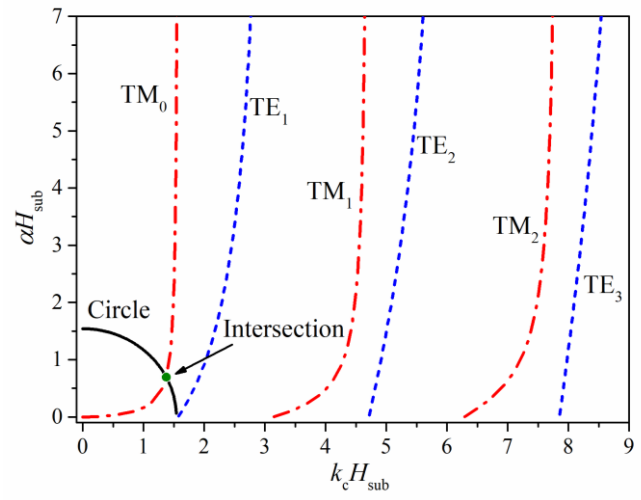

Fig. 2. Graphical solution for the TE and TM surface wave modes on a grounded MgO substrate (ε_r = 9.63 and H_{sub} = 0.3 mm) at 84 GHz.

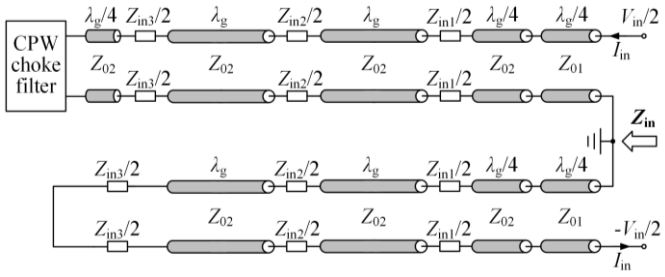

Fig. 3. Equivalent circuit model of the W-band dual-beam lens-free slot-array antenna.

In absence of a dielectric lens, the surface wave modes are inevitably excited due to the high relative permittivity (ε_r = 9.63) and relatively large thickness (H_{sub} = 0.3 mm) of the MgO chip. Considering the antenna structure as shown in Fig. 1, the surface wave excited by each long slot can be approximated as propagating on a grounded substrate. The surface wave equations for the TE and TM modes can be derived as [16]

$$-k_c H_{sub} \cot k_c H_{sub} = \alpha H_{sub} \tag{1}$$

and

$$k_c H_{sub} \tan k_c H_{sub} = \varepsilon_r \alpha H_{sub} \tag{2}$$

respectively, where k_c and α are surface wave propagation constants. Meanwhile, k_c and α should satisfy Eq. (3), i.e.,

$$k_c^2 H_{sub}^2 + \alpha^2 H_{sub}^2 = (\varepsilon_r - 1) k_0^2 H_{sub}^2 \tag{3}$$

where k_0 is the wave number in the free space. Using the variables $k_c H_{sub}$ and αH_{sub}, it can be readily found that Eq. (3) describes a circle while Eqs. (1) and (2) are transcendental equations. By numerical calculations using MATLAB, the graphical solution for the TE and TM surface wave modes is obtained and plotted in Fig. 2. Clearly, only the TM_0 mode can be present in the MgO chip with the given substrate thickness and operating frequency. Hence, those six array elements have been designed to be equally spaced by a half wavelength of the dominant TM_0 mode, thus resulting in a good cancellation and suppression of the unwanted surface wave radiations.

Considering the low normal resistance (with values typically in the range of 2-8 Ω) of the superconducting Josephson junction, impedance matching design is critically important for maximizing the RF and LO coupling efficiencies. Fig. 3 shows the equivalent circuit model of the W-band dual-beam lens-free slot-array antenna. Clearly, the whole antenna structure has been modelled as multiple transmission lines in series with multiple lumped resistors. All transmission lines but the rightmost ones have the same characteristic impedance of Z_{02}. The values of those lumped resistors are equal to half the input impedances at the feeding

point of each long slot in presence of mutual coupling. According to the circuit model as shown in Fig. 3, the input impedance of the whole antenna can be derived as

$$Z_{\text{in1}} = \frac{V_{\text{in}}}{2I_{\text{in}}} = \frac{Z_{01}^2}{Z_{02}^2}\left(\frac{Z_{02}^2}{Z_{\text{filter}}} + Z_{\text{in3}} + Z_{\text{in2}} + Z_{\text{in1}}\right) \quad (4)$$

$$Z_{\text{in2}} = \frac{V_{\text{in}}}{2I_{\text{in}}} = \frac{Z_{01}^2}{Z_{02}^2}\left(Z_{\text{in3}} + Z_{\text{in2}} + Z_{\text{in1}}\right) \quad (5)$$

$$Z_{\text{in}} = Z_{\text{in1}} + Z_{\text{in2}} \approx 6Z_{01}^2 Z_{\text{inx}} / Z_{02}^2 \quad (6)$$

where the term $Z_{02}^2 / Z_{\text{filter}}$ is ignored due to the high choke filter impedance at the operating frequency, and the impedances Z_{in1}, Z_{in2}, and Z_{in3} are considered to have the same value (denoted as Z_{inx}). Hence, the input impedance Z_{in} of the antenna can be optimized by adjusting the parameters Z_{01}, Z_{02} and Z_{inx}.

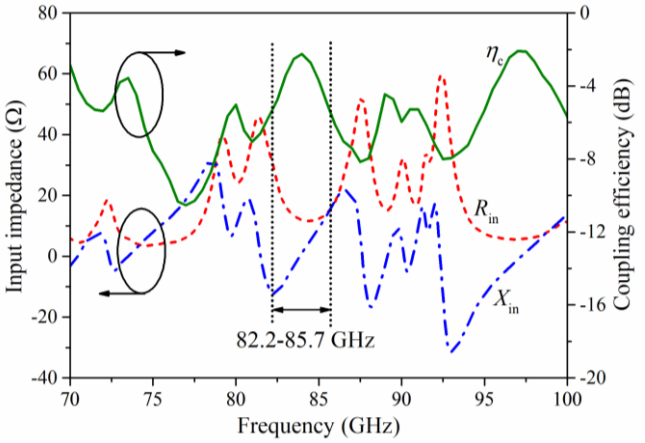

Fig. 4. Simulated input impedance and coupling efficiency of the W-band dual-beam slot-array on-chip antenna.

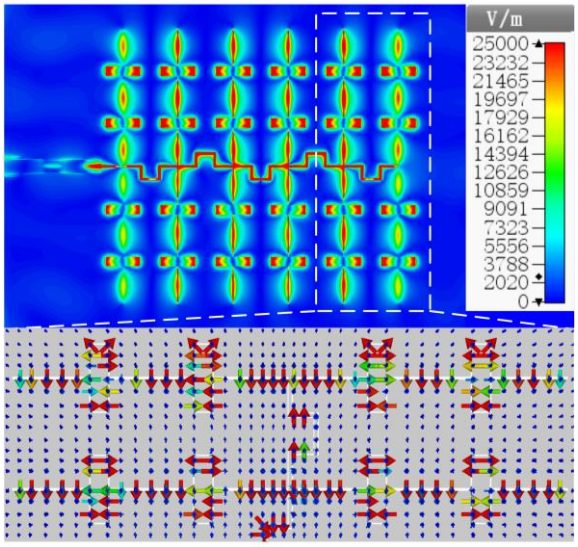

Fig. 5. Simulated surface electric current distribution on the W-band dual-beam slot-array antenna.

Electromagnetic simulation is carried out for the presented antenna using the software Computer Simulation Technology Microwave Studio. Fig. 4 shows the simulated input impedance and coupling efficiency with the operating frequency. It clearly shows that the input resistance is only 12 Ω at a resonant frequency of 84 GHz, which accordingly minimizes the mismatch loss for the slot-array antenna and superconducting Josephson junction at the band. The coupling efficiency η_c of the antenna is defined as [11]

$$\eta_c = \left(1 - |S_{11}|^2\right)\eta \quad (7)$$

where S_{11} is the reflection coefficient and η is the radiation efficiency, respectively. It is found that the coupling efficiency achieves a peak value of -2.2 dB at 84 GHz and the available 3-dB bandwidth is from 82.2 to 85.7 GHz, which indicates a relatively good RF coupling over the band.

Fig. 5 shows the simulated surface electric current distribution at the operating frequency of 84 GHz. Clearly, all array elements are excited in phase by using the CPW meander lines with length of one effective wavelength. For each antenna element, the electric current vectors are in same direction for the straight slot sections while reversed for the rectangular loops (as shown in the inset of Fig. 5). As a result, all the electric currents on the antenna together contribute to good broadside radiations. In addition, the RF currents are well prevented from leaking into the dc/IF port, which indicates the good isolation performance of the fourth-order CPW choke filter.

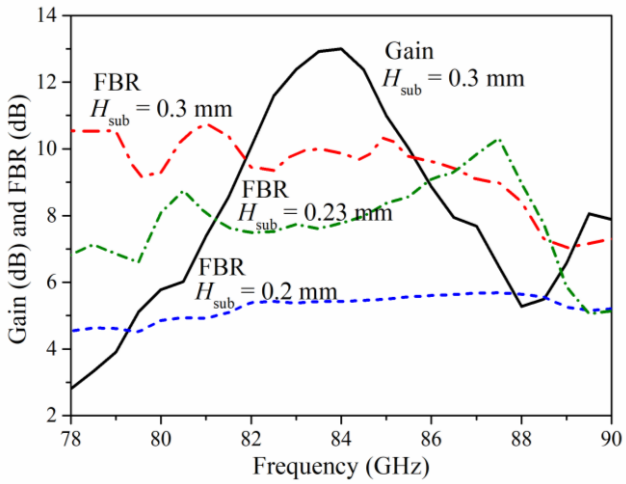

Fig. 6. Simulated gain and FBR of the slot-array antenna with the operating frequency.

The relationship of antenna gain with operating frequency is shown in Fig. 6. Featuring such a lens-free slot-array radiating structure, the antenna exhibits a relatively high gain of around 13 dB at the band of interest. Fig. 7 shows the simulated radiation patterns in the XZ and YZ planes at the frequencies of 82.2 GHz, 84 GHz and 85.7 GHz,

respectively. Clearly, the antenna exhibits typical dual-beam radiation characteristics, which can be readily understood considering the absence of dielectric lens. Furthermore, the back-lobe level is 10 dB lower than that of the main beam, which can be optimized by tuning the substrate thickness. As shown in Fig. 6, the front-to-back ratio (FBR) rises with increasing H_{sub} from 0.2 mm to 0.3 mm. The reason is due to that H_{sub} = 0.3 mm corresponds to approximately quarter effective wavelength in the MgO substrate, which enhances power reflection from the top metal layer and thus results in a relatively low back-lobe level. The main and back lobes are utilized for coupling the RF and LO signals in opposite directions, respectively. It should be emphasized that such asymmetrical dual-beam radiation is advantageous for minimizing the RF coupling loss while absorbing sufficient LO power for pumping the superconducting receivers. As clearly shown in Fig. 7, all co-polarized radiation patterns exhibit high directivity along the positive and negative Z directions, with good radiation symmetry for the main and back lobes in the XZ and YZ planes. Besides, the side-lobe and cross-polarization levels are all below -12 dB and -23 dB, respectively.

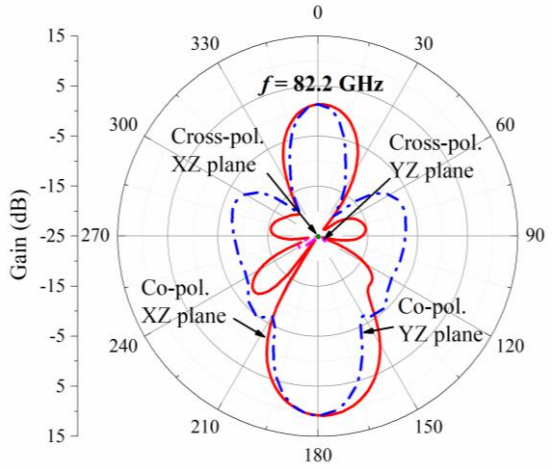

(a)

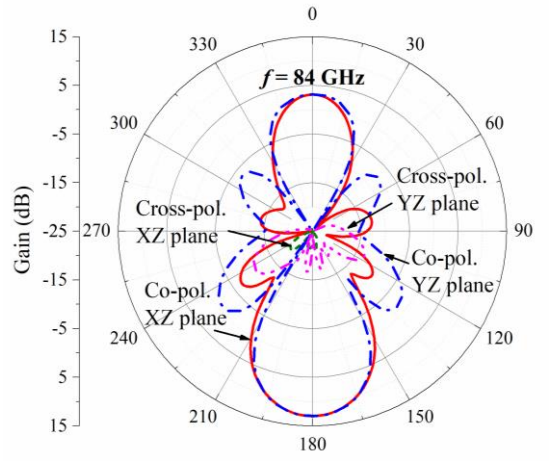

(b)

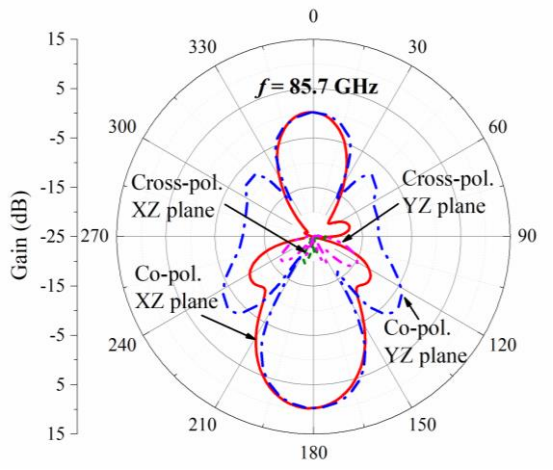

(c)

Fig. 7. Simulated radiation patterns of the slot-array antenna at the frequencies of (a) 82.2 GHz, (b) 84 GHz and (c) 85.7 GHz, respectively.

3. W-band HTS fundamental mixer coupled using the dual-beam slot-array antenna

3.1 Mixer implementation and experiment setup

A W-band HTS Josephson fundamental mixer coupled with the presented dual-beam slot-array antenna was developed at the CSIRO laboratory using the advanced YBCO step-edge Josephson junction technology [17, 18]. As shown in the inset of Fig. 8, a step-edge grain boundary junction has been integrated at the port of the slot-array antenna. The junction was created by etching a step pattern on a 0.3 mm thick MgO (100) substrate, followed by the YBCO film deposition and patterning using a standard photolithography and Ar-ion beam etching techniques. The slot-array antenna with the CPW isolation network is patterned on a 300 nm thick gold thin film (the yellow-colored part). The YBCO lines beneath the gold film connect the Josephson junction for dc biasing and measuring the dc current-voltage characteristics (IVCs) of the junction.

The HTS mixer chip with size of 10×10 mm^2 was packaged and located at the center of a well-designed house (see Fig. 8). Besides, a bias-tee network has been designed to ensure that there is sufficient isolation between the dc biasing applied to the Josephson junction and the IF signal output from the HTS mixer chip. The three-port bias-tee circuit, implemented on a 0.254 mm thick Alumina substrate, consists of a 100 nF series capacitor used to block the dc signal from the IF port and a resistor-capacitor network that acts as a low-pass filter to prevent the IF signal from leaking into the dc port. Furthermore, two 500 Ω resistors were connected on the dc lines for IVC measurement of the Josephson junction. The overall dimensions of the bias-tee circuit are 10 mm x 5 mm. The bias-tee network has very good performance, of which the reflection coefficients at the IF and dc/IF ports are lower than -18 dB, and the

transmission coefficient between those two ports is higher than -1 dB over a frequency range from 1 to 8 GHz.

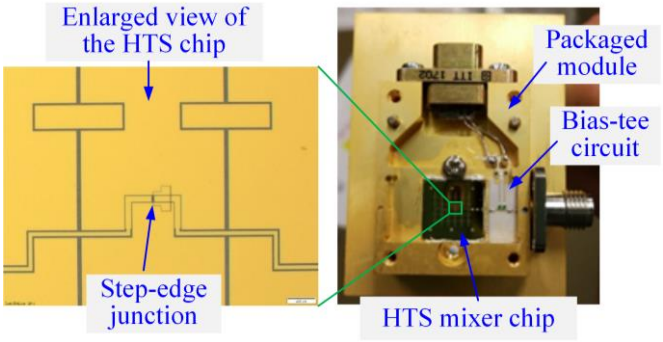

Fig. 8. Photograph of a packaged W-band HTS fundamental mixer module that integrates a HTS mixer chip and a bias-tee circuit. The inset is an enlarged view of the HTS chip showing the YBCO step-edge Josephson junction and a part of the slot-array antenna.

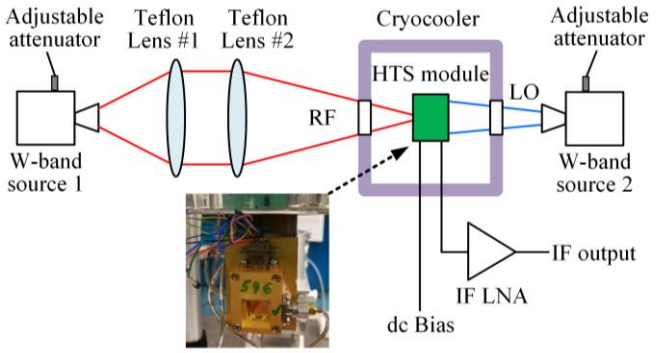

Fig. 9. Schematic diagram of the experimental setup for characterizing the W-band HTS fundamental mixer prototype coupled with the dual-beam slot-array antenna. The inset shows the packaged mixer module mounted onto the coldhead of a cryocooler.

Fig. 9 shows the schematic diagram of an experimental set-up for characterizing the W-band HTS fundamental mixer prototype. Benefiting from the dual-beam radiation properties of the lens-free slot-array antenna, the RF and LO signals can be coupled through two windows into the HTS mixer module mounted in a temperature adjustable cryocooler [19]. Two Rohde&Schwarz frequency multipliers (i.e., R&S SMZ90 and R&S SMZ110) [20], together with two Millitech SGH-12 horn antennas [21], were utilized to generate the required RF (78-90 GHz) and LO (84 GHz) radiations, respectively. To minimize the RF link loss, two Teflon plano-convex lens were used to collimate and focus the radiation beam into the HTS mixer module. Considering the low LO power required for pumping the HTS mixer, no quasi-optics component was used in the LO link. Under an appropriate dc bias provided by a battery-operated current source, heterodyne mixing occurs between the RF and LO signals. The frequency down-converted IF signal was amplified by a Mini-circuits ZVA 213+ low noise amplifier with gain of ~26 dB [22], and then recorded using an Keysight spectrum analyzer. In addition, two adjustable attenuators were utilized to have the HTS mixer operate within its linear region and to optimize the LO pumping power for maximizing the mixer performance, respectively.

3.2 Measurement and simulation results

The W-band HTS mixer prototype was measured at the operating temperatures of 20 K, 40 K and 60 K, respectively. Fig. 10(a) and 10(b) show the measured dc IVCs when unpumped and pumped with a LO signal, respectively. Considering the junction capacitance is extremely small for HTS step-edge junctions, the unpumped IVCs display typical resistively-shunted-junction (RSJ) behavior. The junction normal resistance R_n (the slope of the linear section) and critical current I_c (maximum zero-voltage currents) can be readily estimated from the characterized IV curves. It is found that the measured normal resistance R_n is around 2.1 Ω, and the critical current I_c is 360 μA, 240 μA and 120 μA at the temperatures of 20 K, 40 K and 60 K, respectively. As shown in Fig. 10(b), the junction critical currents are suppressed by a LO pumping signal at the frequency of 84 GHz. By measuring the LO induced I_c suppression plus deducting the antenna-junction mismatch loss, the LO power P_{LO} was obtained to be around -47 dBm. Fig. 10(b) also shows a series of Shapiro steps appearing at equally spacing voltages, which can be well predicted from the Josephson voltage-frequency relationship [23]. In addition to experimental characterizations, numerical simulations were also carried out using the three-port method [24, 25], where the measured values of R_n, I_c and P_{LO} were imported into the parametric simulation model. As shown in Fig. 10, all simulated results agree well with the measured results, with very minor difference resulting from the experiment errors.

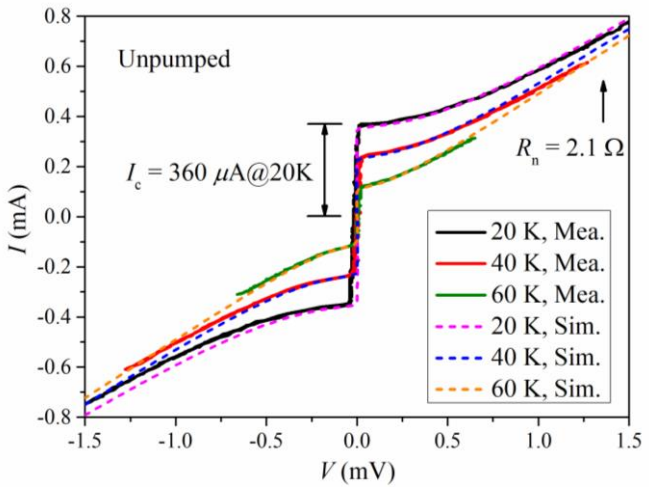

(a)

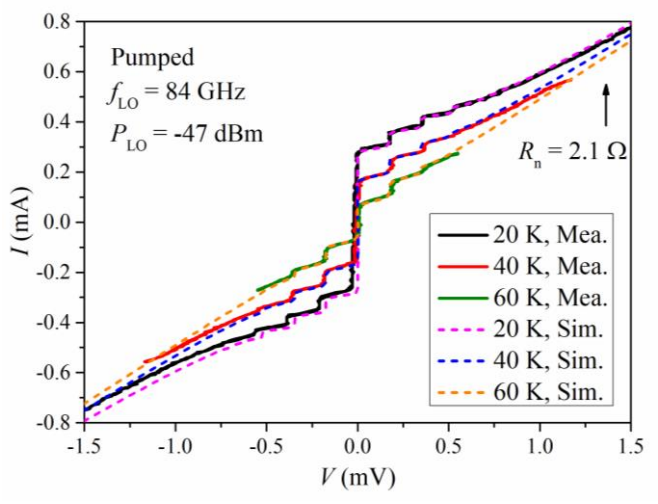

(b)

Fig. 10. Measured and simulated dc IVCs of the W-band HTS mixer at different operating temperatures when (a) unpumped and (b) pumped with a LO signal.

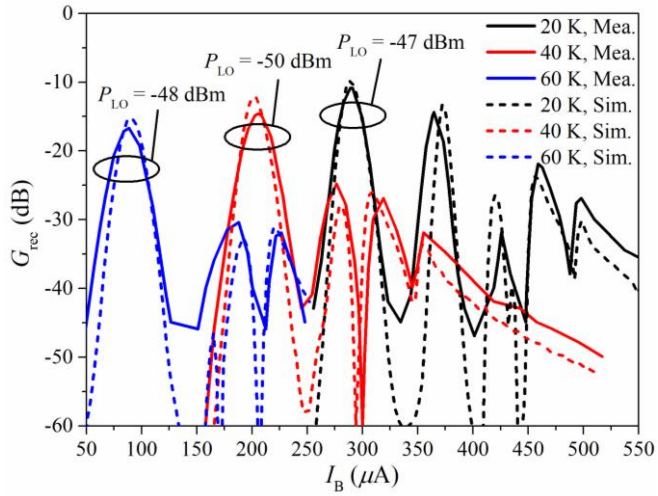

Fig. 11. Measured and simulated conversion gain G_{rec} versus bias current I_B for different operating temperatures.

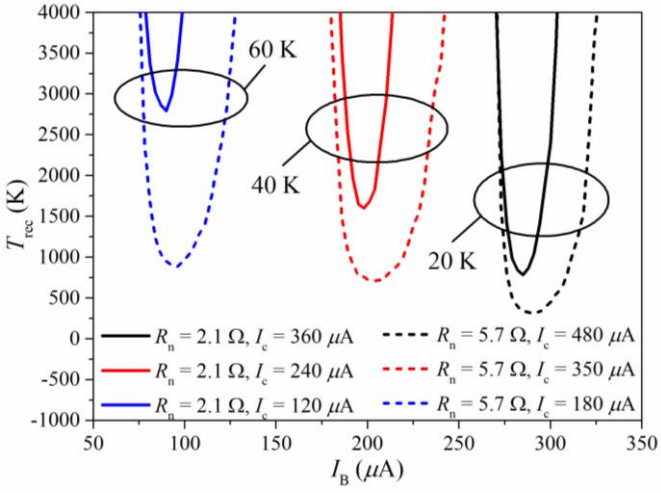

Fig. 12. Simulated noise temperature T_{rec} versus bias current I_B for different operating temperatures.

Fig. 11 shows the measured and simulated conversion gain G_{rec} versus bias current I_B for different operating temperatures. The RF and LO signal frequencies were set to be 85 GHz and 84 GHz, respectively. The conversion gain G_{rec} was obtained from $G_{rec} = P_{IF} / P_{RF} / G_{IF}$, where G_{IF} is the calibrated IF link gain, P_{IF} is the measured IF output power using the spectrum analyzer and P_{RF} is the RF input power measured in the same way as that for P_{LO} estimation, respectively. It is seen that G_{rec} is dependent on I_B with multiple peaks appearing, which can be readily understood from the pumped dc IVCs as shown in Fig. 10(b). The peaks are achieved when I_b is located halfway between adjacent Shapiro steps, where the dynamic resistance R_D (i.e., the slope of the IV curve) reaches the maximum. Considering lower critical current and smaller dynamic resistance were observed for higher operating temperature, the G_{rec} peaks move leftward and decline with increasing the operating temperature (see Fig. 11). Due to the difference in pumped dc IVCs, the LO power P_{LO} was slightly adjusted for different operating temperatures, which are -47 dBm for 20 K, -50 dBm for 40 K and -48 dBm for 60 K, respectively. Moreover, the simulated and measured results agree very well in terms of the curve shape, peak position, and G_{rec} values. The measured best G_{rec} is -10 dB at 20 K, -14.6 dB at 40 K and -16.7 dB at 60 K, respectively. Some minor differences between the simulation and experimental results are attributed to the measurement and calibration errors in our experiment.

Due to the lack of MMW blackbody, filter and other necessary quasi-optical components with sufficiently large aperture, we have not yet established the experimental setup for the mixer noise characterization at W-band. Fig. 12 shows the simulated noise temperature T_{rec} versus bias current I_B for different operating temperatures. Similar to the relationship between G_{rec} and I_B, the peak T_{rec} value rises and the optimum I_B location moves leftward with increasing the operating temperature. The best noise temperature for the fabricated mixer protype is around 780 K at 20 K, 1600 K at 40 K and 2790 K at 60 K, respectively. In this study, the junction parameters were less optimal, i.e., the I_c, R_n and thus I_cR_n values were lower than ideal ones. It is expected that the mixer performance should be significantly improved if better Josephson junction parameters were acquired. Applying our previous experimental R_n and I_c values for the 340-GHz HTS mixer module [26], we show that in Fig. 12, the mixer noise temperature can be reduced to 310 K at 20 K, 700 K at 40 K and 880 K at 60 K, respectively.

Table 1: Performance Comparison of State-of-the-Art HTS Fundamental Mixers at Similar Operating Frequencies

References	Operating frequency	Operating temperature	Conversion gain	Noise temperature

[5]	100 GHz	4.2 K	-	2800 K
[6]	94 GHz	10 K	-7.6 dB	3400 K
[7]	90 GHz	20 K	-10 dB	1600 K
[8]	70 GHz	58 K	-37 dB	-
This work	**84 GHz**	**20 K**	**-10 dB**	**780 K**
		40 K	**-14.6 dB**	**1600 K**
		60 K	**-16.7 dB**	**2790 K**

Table 1 compares the performance of the presented mixer device with other state-of-the-art HTS fundamental mixers operating at similar frequencies. Compared to Refs. [5-7], our mixer exhibits a superior noise performance and the capability of operating at higher temperatures. Compared to Ref. [8], the presented mixer has a considerably higher conversion gain. Moreover, it should be pointed that the device performance can be further improved if better Josephson junction parameters could be obtained. The results have validated the concept of design and the good performance of the W-band HTS fundamental mixer coupled using a dual-beam lens-free slot-array antenna.

4. Conclusion

We have presented a dual-beam lens-free slot-array antenna coupled HTS mixer operating at the W-band. The antenna exhibits high coupling efficiency for superconducting Josephson junctions and enables asymmetric dual-beam radiations in opposite directions, thus not only reducing the RF coupling losses but greatly facilitating the quasi-optics design for cryogenic receiver integration. Based on the designed antenna, a HTS fundamental mixer protype has been developed and characterized at different operating temperatures. The experimental and simulation results have shown the good device performance. The measured conversion gain is -10 dB at 20 K, -14.6 dB at 40 K and -16.7 dB at 60 K, respectively. The noise temperature is predicted to be around 780 K at 20 K, 1600 K at 40 K and 2790 K at 60 K, respectively. These results are superior to other state-of-the-art HTS mixers reported in literature at similar operating frequencies.

Lastly, it should be emphasized that the dual-beam lens-free slot-array antenna is applicable to not only the HTS receivers but also LTS counterparts. The device will find huge potential in MMW communication, imaging, and astronomical applications.

Acknowledgments

This work was supported by the CSIRO Space Future Science Program Project (No. ST-R2-03). A part of this work was also supported by the National Key Research and Development Program of China (No. 2019YFB1803200) and the National Natural Science Foundation of China (No. 62171032, No. 61620106001). The authors would like to thank our CSIRO colleagues Ms. Jeina Lazar for the HTS chip fabrication and Mr. Ken Smart for assistance in experimental setup.

References

[1] Mehrpouyan H, Khanzadi M R, Matthaiou M, Sayeed A M, Schober R and Hua Y 2014 Improving bandwidth efficiency in E-band communication systems *IEEE Commun. Mag.* **52** 121-128

[2] Yang G, Li C, Gao H, Li H, Zheng S and Fang G 2021 Efficient phase shift migration for MIMO 2-D imaging in millimeter-wave band *IEEE Microw. Wirel. Compon. Lett.*, **31** 215-218.

[3] Shan W, Yang J, Shi S, Yao Q, Zuo Y, Lin Z, Chen S, Zhang X, Duan W, Cao A, Li S, Li Z, Liu J and Zhong J 2012 Development of superconducting spectroscopic array receiver: a multibeam 2SB SIS receiver for millimeter-wave radio astronomy *IEEE Trans. THz Sci. Technol.* **2** 593-604.

[4] Wei H-J, Meng C, Wang T-W, Lo T-L and Wang C-L 2012 60-GHz dual-conversion down-/up-converters using schottky diode in 0.18 μm foundry CMOS technology *IEEE Trans. Microw. Theory Tech.* **60** 1684-1698

[5] Shimakage H, Uzawa Y, Tonouchi M and Wang Z 1997 Noise temperature measurement of YBCO Josephson mixers in millimetre and submillimeter waves *IEEE Trans. Appl. Supercond.* **7** 2595-2598

[6] Harnack O, Darula M, Andoh H, Beuven S and Kohlstedt H 1999 Noise and mixing properties of high-Tc Josephson junctions at W-band frequencies *Appl. Supercond.* **6** 689-697

[7] Harnack O, Darula M, Scherbel J, Heinsohn J K, Siegel M, Diehl D and Zimmermann P 1999 Optimization of a 115 GHz waveguide mixer based on an HTS Josephson junction *Supercond. Sci. Technol.* **12** 847-849

[8] Malnou M, Feuillet-Palma C, Ulysse C, Faini G, Febvre P, Sirena M, Olanier L, Lesueur J and Bergeal N 2014 High-Tc superconducting Josephson mixers for terahertz heterodyne detection *J. Appl. Phys.* **116** 074505

[9] Zhang T, Pegrum C, Du J and Guo Y J 2016 Simulation and measurement of a Ka-band HTS MMIC Josephson junction mixer *Supercond. Sci. Technol.* **30** 015008

[10] Zhang T, Gao X, Wang W, Du J, Pegrum C and Guo Y J 2017 A 36 GHz HTS MMIC Josephson mixer – simulation and measurement *IEEE Trans. Appl. Supercond.* **27** 1502405

[11] Gao X, Zhang T, Du J, Weily A R, Guo Y J and Foley C P 2017 A wideband terahertz high-T_c superconducting Josephson-junction mixer: electromagnetic design, analysis and characterization *Supercond. Sci. Technol.* **30** 095011

[12] Focardi P, McGrath W R and Neto A 2005 Design guidelines for terahertz mixers and detectors *IEEE Trans. Microw. Theory Tech.* **53** 1653-1661

[13] Du J, Weily A R, Gao X, Zhang T, Foley C P and Guo Y J 2016 HTS step-edge Josephson junction terahertz harmonic mixer *Supercond. Sci. Technol.* **30** 024002

[14] Gao X, Du J, Zhang T and Guo Y J 2019 High-Tc superconducting fourth-harmonic mixer using a dual-band terahertz on-chip antenna of high coupling efficiency *IEEE Trans. THz Sci. Technol.* **9** 55-62

[15] Gao X, Zhang T, Du J and Guo Y J 2018 300-GHz dual-beam frequency-selective on-chip antenna for high-Tc superconducting receivers *Proc. 2018 Int. Symp. Antennas Propag. (Korea: Pusan).*

[16] Pozar D M 2011 *Microwave Engineering* (New York: Wiley)

[17] Foley C P, Mitchell E E, Lam S K H, Sankrithyan B, Wilson Y M, Tilbrook D L and Morris S J Fabrication and characterisation of YBCO single grain boundary step edge junctions 1999 *IEEE Trans. Appl. Supercond.* **9** 4281-4284
[18] Mitchell E E and Foley C P 2010 YBCO step-edge junctions with high I_cR_n *Supercond. Sci. Technol.* **23** 065007
[19] Du J, Macfarlane J C, Lam S H K and Taylor R T 2009 HTS Josephson heterodyne oscillator on a pulse-tube cryocooler *Supercond. Sci. Technol.* **22** 105013
[20] R&S SMZ90 and R&S SMZ110 (available at: www.rohde-schwarz.com)
[21] SGH-12 (available at: www.amtechs.co.jp/product/IS000025-SGH.pdf)
[22] ZVA 213+ (available at: www.mini-circuits.com)
[23] Duzer T V and Turner C W 1999 *Principles of Superconductive Devices and Circuits* (Upper Saddle River, NJ: Prentice-Hall)
[24] Taur Y 1980 Josephson-junction mixer analysis using frequency-conversion and noise correlation matrices *IEEE Trans. Electron Devices.*, **27** 1921-1928
[25] Gao X, Du J, Zhang T and Guo Y J 2017 Noise and conversion performance of a high-T_c superconducting Josephson junction mixer at 0.6 THz *Appl. Phys. Lett.* **111** 192603
[26] Gao X, Zhang T, Du J and Guo Y J 2020 340 GHz double-sideband mixer based on antenna-coupled high-temperature superconducting Josephson junction *IEEE Trans. THz Sci. Technol.* **10** 21-31